JOINT TIME-FREQUENCY DOMAIN REFLECTOMETRY AND STATIONARITY INDEX FOR WIRE DIAGNOSTICS IN AIRCRAFT

Mokhtar Sadok[1], Mériem Jaidane[2], and Michael Walz[3]

(1) Mokhtar Sadok is a senior scientist at Goodrich Corporation
(2) Mériem Jaidane is a professor at Unité Signaux et Systèmes of Ecole Nationale d'Ingénieurs de Tunis
(3) Michael Walz is the manager of the FAA Aging Aircraft Electrical Systems Program

Abstract

This paper proposes a new technique for wire diagnostics based on joint time-frequency analysis. The Continuous Wavelet Transform (CWT) is used to generate time-frequency maps while a staionarity index is used to interpret such time-frequency representation. Signals are generated using a high bandwidth Time Domain Reflectometry (TDR) device.

The stationarity index is used as a direct indicator of defects in the wire under test. The index stays low if there is no defect but jumps suddenly if a defect is encountered. The detection method consists of comparing measures of the same global Time Frequency Representation (TFR) taken at different instants in the time-frequency plan, where time is equated with distance. The global TFR is computed over the entire frequency span of the signature under test.

The proposed approach has been applied to a database of wire signatures collected via the Goodrich Wire Integrity Tool (GWIT), a hand held TDR of 200 Pico second rise time and 2.5 GHZ bandwidth. Three different locations are used to collect data subject of this study. Data is collected at the Goodrich engineering lab in Vermont, at Sandia Lab in New Mexico, and over a Boeing 737 airplane at the FAA Tech Center in New Jersey.

The detection algorithms are coded and implemented in the Goodrich hand held TDR. The unique input to the system is the TDR waveform; no other properties of the wire are required including wire type, gauge, or length.

1. Background

Wire diagnostics has become a vital maintenance component to improve aircraft safety and readiness. Recent inspection of aging aircraft has uncovered a major role played by aircraft wiring systems in aircraft downtime. Some aircraft catastrophic incidents, such as the Swiss Air 111 in 1998, have been directly linked to wire problems. As such, an efficient solution for wire diagnostic is highly desirable. The FAA has been steadily encouraging research in this area. This study is funded by the FAA and is undertaken by Goodrich in response to a Broad Agency Announcement (BAA) to advance the Development of Electrical Wiring Interconnect System Test and Inspection Systems.

Single wires are, by far, the most challenging type of wires for diagnosis mainly because of the uncontrolled distance between the wire and its return path. Distance between the wire under test and its return path affects the wire impedance, particularly when operating at high frequency. The distance between the wire and its return path in the case of single wires is expected to vary from one point over the wire to another given the anticipated bending and movement of wires. This is what makes single wires hard to diagnose. A system capable of adequately diagnosing single wires is expected to perform even

better in the case of other types of wires. A specific study to quantify the effect of distance variation on the TDR-based diagnosis of single wires has been submitted for publication elsewhere [1].

Current techniques for wire inspection are based on the concept of Reflectometry [2-3]. One of the big advantages of Reflectometry-based techniques is that it requires connection to only one end of the wire. Most common Reflectometry techniques are either based on time domain (Time Domain Reflectometry, TDR) or on frequency (Frequency Domain Reflectometry, FDR). This paper attempts to take advantages of both domains and proposes detection techniques based on joint Time-Frequency Domain Reflectometry (TFDR).

2. Time-Frequency Domain Algorithms

Wavelets are used to provide time-frequency maps for TFDR analysis. Hilbert Huang Transform is another time-frequency technique that was studied during this project. Finding of such a study is published in this conference as well [4].

Wavelet transform is computed by projecting the signal of interest into a particular basis that is formed by dilating and translating a unique function commonly termed as the mother wavelet. Wavelet analysis depends heavily on the mother wavelet function. Different mother wavelets are appropriate for different applications. The mother wavelet is typically chosen such that the associated digital filter has a small order (to speed up the convolution) and such that the resulting analysis yields only few nonzero coefficients. This is criterion is mostly relevant in data compression. For the application at hand, the interest is in selecting a mother wavelet that resembles most embedded features in the TDR signature. Several types of wavelets such as Daubechies, Meyer, Morlet, Mexican hat, Symlets, and Biorthogonal wavelets have been tested. The Mexican hat wavelet is found to be most effective in extracting defect-related features in TDR signatures; most likely because of the Gaussian nature of this wavelet function that resembles several high frequency natural artifacts. Implementing and testing the Mexican-hat based wavelet transform constitute the first major part of the TFDR algorithms.

The second part of the TFDR algorithms addresses the interpretation of the wavelet-based time-frequency representation. A Stationarity Index (SI) is used as a direct indicator of defects in the wire under test [5]. The index stays very low if there is no defect but jumps suddenly if a defect is encountered. The detection method consists of comparing measures of the same global Time Frequency Representation (TFR) taken at different instants in the time-frequency plan, where time is equated with distance. The stationarity index approach is based on interpreting the time-frequency plan as a two-dimensional probability distribution function already established in the literature. The formal analogy between Time-Frequency Representations (TFRs) and two-dimensional probability density functions has been previously addressed [6-7]. The analogy is drawn under the assumptions of total energy conservation and marginal properties in the TFR. Following is the mathematical foundation of the Mexican hat-based continuous wavelet transform and the stationarity index method.

2.1. Wavelet Transform

Let the "mother wavelet" function be noted $\psi(t)$. The continuous wavelet transform of a function $f(t) \in L^2(R)$ (i.e. space of finite energy functions) is defined as:

$$W_f(a,b) = \rangle f(t), \psi_{ab}(t)\langle = \frac{1}{|a|^{1/2}} \int_{-\infty}^{+\infty} f(t)\psi^*(\frac{t-b}{a})dt \qquad (1)$$

where, $\psi_{ab}(t) = \psi(\dfrac{t-b}{a})$ and $\psi^*(t)$ stands for the conjugate of $\psi(t)$. The variable "a" represents the time information while the variable "b" represents the scale information that is inversely proportional to the frequency information. For $\psi(t)$ to be a wavelet function, it has to meet the following condition [8]:

$$C_h = \int_{-\infty}^{+\infty} \frac{|\Psi(w)|^2}{|w|} dw \prec \infty \tag{2}$$

Where $\Psi(w)$ is the Fourier transform of the mother wavelet $\psi(t)$. The original signal f(t) can be then reconstructed from its wavelet transform:

$$f(t) = \frac{1}{C_h} \int_{-\infty}^{+\infty} \frac{1}{a^2} \int_{-\infty}^{+\infty} W_f(a,b)\psi_{ab}^*(t)\,db\,da \tag{3}$$

For the application at hand, the mother wavelet function, $\psi(t)$, that satisfies both Equations (1) and (2) is given by:

$$\Psi(t) = \left(\frac{2}{\sqrt{3}}\pi^{-\frac{1}{4}}\right)\left(1-t^2\right)e^{-t^2/2} \tag{4}$$

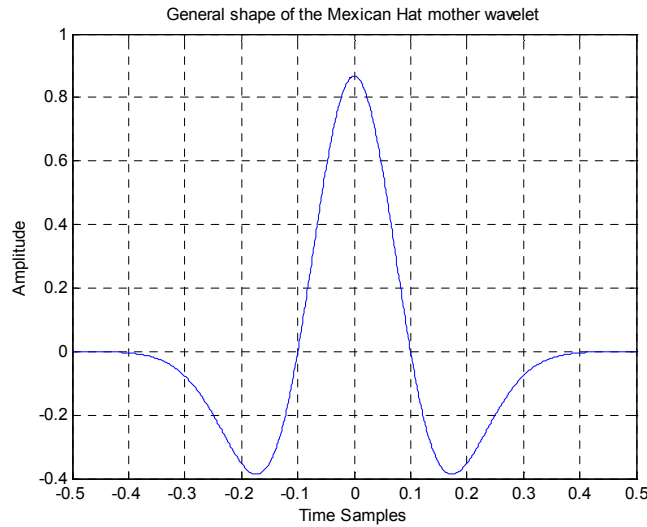Equation 4 defines the Mexican hat mother wavelet while Figure 1 shows its general shape.

Figure 1. General shape of the Mexican-hat wavelet function.

2.2. Stationarity Index

Formal analogy between Time-Frequency Representations (TFRs) and two-dimensional probability density functions is drawn under the assumptions of total energy conservation and marginal properties in the TFR, respectively, illustrated by Equations 5-6 [6-7]:

$$\text{Energy conservation:} \iint C_s(t,f)\,dt\,df = \int |s(t)|^2\,dt \tag{5}$$

$$\text{Marginal properties:} \begin{cases} \int C_s(t,f)df = |s(t)|^2 \\ \int C_s(t,f)dt = |S(f)|^2 \end{cases} \tag{6}$$

Where $S(f)$ and $C_s(t,f)$ are respectively the Fourier transform and the time-frequency distribution of the time signal $s(t)$ in the selected Time Frequency Representation (TFR). Most of the classical and new TFRs fulfil these conditions. Examples of such TFRs include the Spectrogram (also known as the Short-Fourier Transform), wavelets, and the Huang Hilbert Transform (HHT) [6]. Similarity between classical 2-D probability theory and TFR expressed by Equations 5-6 motivates the use of Shannon entropy to measure the information content of signals in the time frequency plane [7]. Let a given TFR of a unit energy signal be named $I(t,f)$. Hence, the Shannon entropy of such a TFR is given by:

$$H(I) = -\int\int I(t,f)\log_2 I(t,f)dtdf \tag{7}$$

Standard quality criterion of TFRs is good time-frequency localization. However, for the application at hand, a TFR abruptly varying along the time axis if a change occurs and remaining constant otherwise is the best choice, regardless of its frequency accuracy. In the particular case of wire diagnostics, the time-axis is directly equated with distance. Various time-frequency based distance and divergence measures were proposed in [5] to detect abrupt spectral changes in speech and other synthesized nonstationary signals for classification purposes [7]. At each instant n, two sub-images $I_1(n;\tau,f)$ and $I_2(n;\tau,f)$ with equal time-frequency dimensions (i.e. p by f) are extracted from the global TFR as illustrated by Figure 2
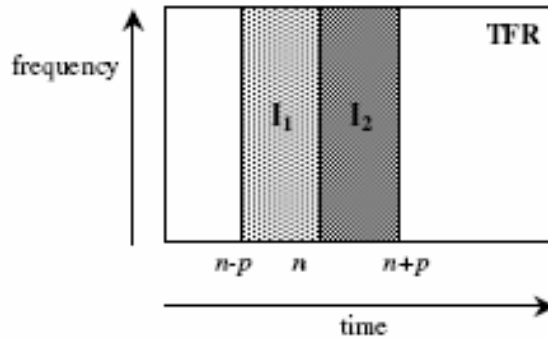

Figure 2. Sub-images I_1 and I_2 of the global TFR at the instant n

The parameter p is the duration of each sub-image. Both sub-images are normalized to have unit energy as follows:

$$NI_k(n;\tau,f) = \frac{|I_k(n;\tau,f)|}{\int_{\tau=0}^{p}\int_{-\infty}^{\infty}|I_k(n;\tau,f)dfd\tau|} \quad k=1,2 \tag{8}$$

The two normalized sub-images separated along the frequency axis at the instant n, are then compared by using a distance measure, as is the case in classical 2-D probability distributions. The choice of the couple (distance measure, TFR) is crucial for an efficient SIT application. The following three distance measures, borrowed from probability theory, have been investigated during this study:

$$\textbf{Kolmogorov distance:}\quad SI_{ko}(n) = \int\limits_{\tau=0}^{p}\int_{-\infty}^{\infty}\left|NI_1(n;\tau,f) - NI_2(n;\tau,f)\right|dfd\tau \qquad (9)$$

$$\textbf{Küllback distance:}\quad SI_{ku}(n) = \int\limits_{\tau=0}^{p}\int_{-\infty}^{\infty}(NI_1(n;\tau,f) - NI_2(n;\tau,f)).\log\left(\frac{NI_1(n;\tau,f)}{NI_2(n;\tau,f)}\right)dfd\tau \qquad (10)$$

$$\textbf{Bhattacharyya distance:}\quad SI_{bh}(n) = -\log\left(\int\limits_{\tau=0}^{p}\int_{-\infty}^{\infty}\sqrt{NI_1(n;\tau,f).NI_2(n;\tau,f)}\right)dfd\tau \qquad (11)$$

As illustrated by Equations 9-11, the proposed measures are functions only of time- equating to distance. The idea is to observe the evolution of such distance measures over time to look for abrupt changes. The parameter p delimits the time-span at the sides of the instant n under consideration. It allows the tuning of the SIT function to detect different levels of nonstatiorities: higher p values lead to smoother distance measures useful to detect subtle changes while lower p values are useful for detecting abrupt changes.

3. Detection approach

The TFDR-based algorithms are designed into two parts. The first part of the algorithms detects "hard" defects (i.e. "short", "open", or "end of wire"). The second part of the algorithms detects "soft" or intermediary impedance defects that could be introductory to hard defects subsequently.

After stimulating the wire with a fast pulse and capturing the reflected time-domain signature, a series of processing steps are performed. First, the voltage waveform is normalized in order to set up universal parameters and detection thresholds regardless of the defect or wire properties. Second, the normalized signature is smoothed by a Linear-phase FIR low pass filter designed using least-squares error minimization. Normalization is done by scaling all TDR Voltage samples between 0 and 2. The smoothing process serves two fold to i)detect hard defects and to ii) exclude fluctuations accompanying such major events. This filtering process is applied only when looking for "hard" defects. Third, a continuous wavelet transform is applied using a single scale value to locate the extrema of the transformed signal. Hard faults are characterized by identifying the amplitude and location of the signal extrema in the wavelet domain. Finally, the stationarity index algorithm is run on the normalized, but not filtered, signature to detect "soft" defects.

To make the detection process more efficient and easier to interpret by the user, only one "soft" defect is displayed at the time. The user may make additional measurements to detect other possible "soft" defects. Figures 3-5 illustrate the detection process. Upper plots of Figure 3 show the signal under test before and after being normalized and filtered. The lower plot indicates the detection of a "hard" defect (i.e. "open") around 10 feet, as expected. In the event no "hard" defect is detected, an "end of wire" message is delivered. Once the "hard" event is identified, the second step includes detecting "soft" defects using the Stationarity Index process. Among the three distance measures given by Equations 9-11, Bhattacharyya distance was found most consistent. All SI plots in this papers are generated using the Bhattacharyya distance.

Figure 4 shows the time-frequency map of the original signal of Figure 3. In this particular case, the distance axis is limited to 10 feet where an "open" was already detected. The output of the stationarity index algorithm when applied to the time-frequency map of Figure 4 is shown at the lower subplot of Figure 5. The upper subplot of Figure 5 shows the original TDR signatures with locations of the "hard" defect (in red) and the "soft" defect (in green). The soft defect is detected around 5 feet. In fact, at 4.6 feet about quarter-inch of the single wire coat was stripped. So in this case, the SIT correctly identified the location of the "soft" defect. However, in a different measurement over the same single wire there was a "false alarm" indication at 3.6 feet as shown by Figure 6. In this case, the system still indicates that

location of the "soft" is at 5 feet- as it corresponds to the largest stationarity value. In some other cases the exact location of the "soft" defect may be ill defined. This is expected given the high variability of the return path in the case of single wires.
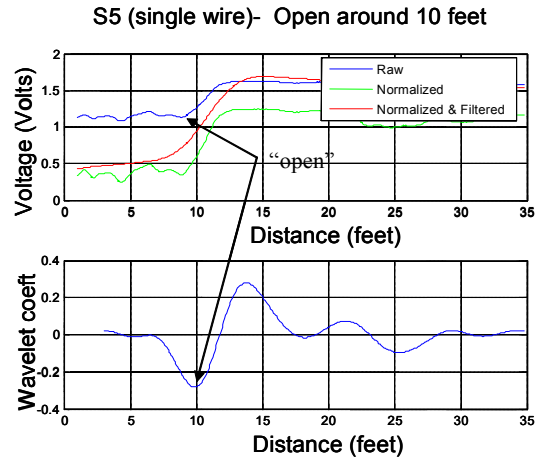

Figure 3. Wavelet-based approach to detect "hard" defects. In this particular case, an "open" is detected on a single wire at 10 feet from the testing point.
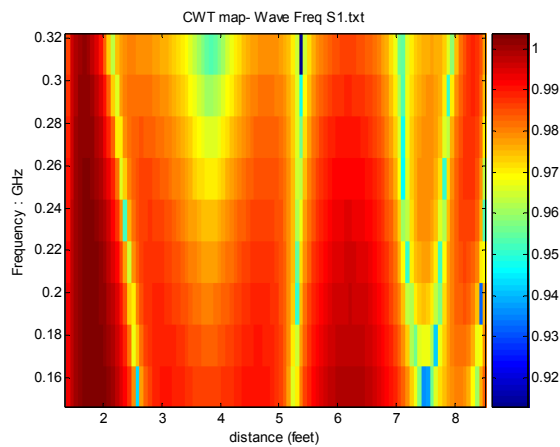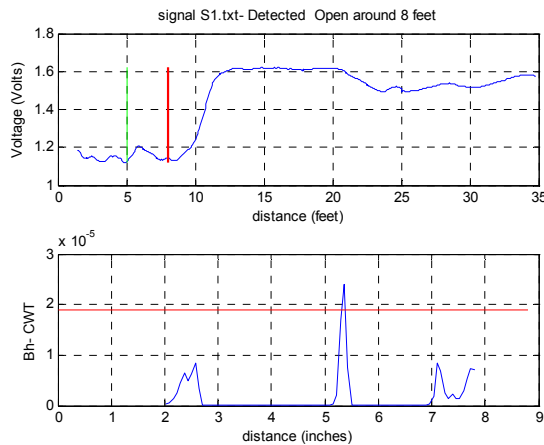

Figure 4. CWT-based Time-Frequency map for "soft" defect detection

Figure 5. "Soft" defect detected at 5.4 feet using the Stationarity Index over the time-frequency map shown at Figure 4. The "soft" defect corresponds to a quarter-inch insulation stripping of a single wire.
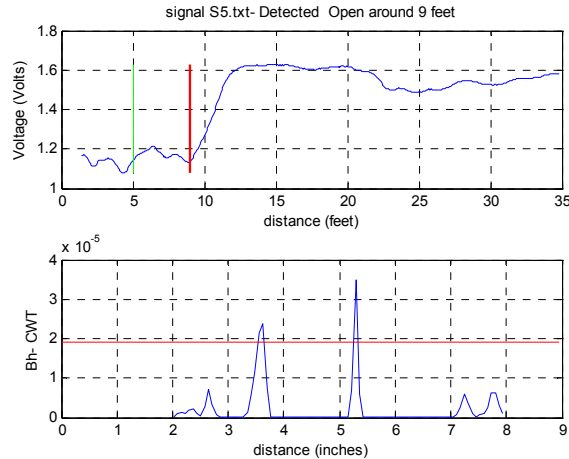
Figure 6. A "false alarm" registered at 3.6 feet after exceeding the detection threshold. The false alarm is exhibited in addition to the "soft" defect already listed at 5.3 feet.

4. Experimental Setup

Data for this study is collected via the Goodrich Wire Integrity Tool (GWIT). The GWIT is built on Pocket PC platform, using a PCMCIA interface. Various tests on the wire are run and warehoused within the Pocket PC for export as a delimited file. The GWIT pulser is in a PCMCIA format with a rise time less than 200 ps and aberrations less than 1%. The ADC is also designed in a PCMCIA format with a 5-Gsps sampling rate. The Windows-based GWIT software has a user friendly interface that is designed to allow maintainers to:

- Generate new wire configurations,
- View current wire test,
- Edit the selected wire test,
- Save results of test,
- Save the current test to baseline,
- Search the database for a test.
- Display information in English and metric units

The wire configuration allows a maintainer to uniquely identify a wire by aircraft, harness and wire within the harness. Figure 7 shows different GWIT maintenance screens available for the user. Figure 8 shows an example of wire shooting via the GWIT.

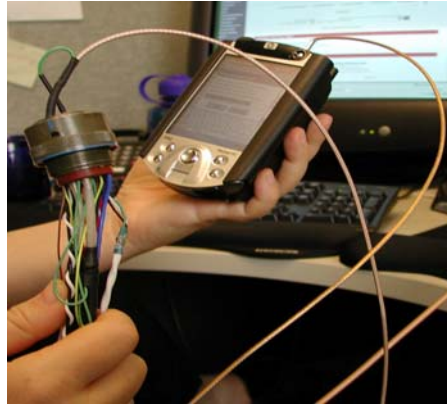**Figure 7. Examples of GWIT maintenance screens**

Figure 8. Wire shooting via the Goodrich Wire Integrity Tool (GWIT) device.

Data has been collected for this study over 3 different locations: Goodrich lab in Vermont, Sandia lab in New Mexico, and the FAA Tech Centre in New Jersey.

Several lab harnesses with various wire types (i.e. single, twisted pair, shielded twisted pair, triple twisted pair, and coaxial) are built at Goodrich engineering lab. Harnesses are built in 10-foot and 20-foot long bundles. Retired harnesses from onboard Goodrich fuel quantity systems are also used testing. Small damages in the order of 1 to 2 cm abrasions are applied to the exterior shield of the wire under test.

A wire test bed at the Airworthiness Assurance Nondestructive Inspection (NDI) Validation Center (AANC), located at Sandia National Laboratories is built with a mission to set standards in defining and testing wire defects over a wide range of conditions. The test bed consists of wire harnesses representative of typical systems found on commercial passenger aircraft. The wire harnesses are contained within a metallic enclosure to simulate typical aircraft structures. There are 11 standard types of wire defects that are identified and studied in this project. Table I lists these defects; for more details see [9].

Defect	Description
DT1	Abraded or chaffed insulation
DT2	Breached Insulation (360° Exposed Conductor)
DT3	Cracked Insulation
DT4	Conductor-Strand Breaks
DT5	Over-pressured Clamps
DT6	Bend Radius
DT7	Faulted Splices
DT8	Heated Insulation
DT9	Conductor Opened
DT10	Conductor Shorted
DT11	Conductor corroded

Table I: List of wire defects as defined by the AANC at Sandia Lab

The GWIT is used to collect TDR waveforms over several harnesses at the avionics bay and the cockpit of a 737 aircraft. No a priori knowledge is available regarding the state of aircraft wires. Figure 9 shows an example of tested harnesses at the avionics bay.
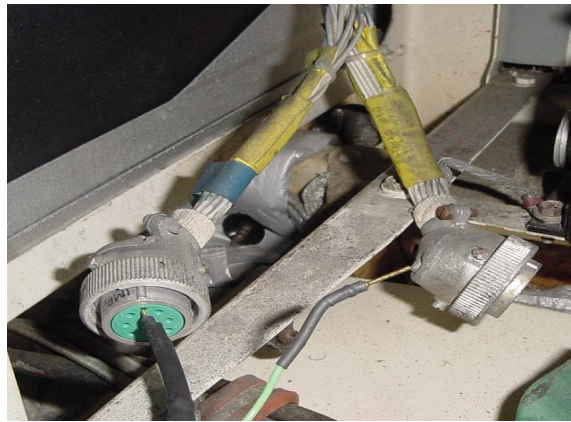

Figure 9. Two tested wire harnesses at the avionics bay of a Boeing 737 aircraft. Pins of each connector are labeled by alphabetical letters "a', "b"…etc

5.   Experimental Results

5.1. Goodrich lab data

A10-foot wire harness is connected, via a connector, to a 20-foot harness to form a 30-foot harness. Figure 10 shows an open detected around 28 feet on the 30-foot harness. Note that the original signal is seen as 29 feet rather than 30 feet. This lack of precision in locating defects is mainly due to the imprecise Velocity Of Propagation (VOP) of electricity inside the wire as the VOP is set at 0.71 for all types of wires. Since the wire type is not required by the system for practical reasons, an average VOP value of 0.71 is adopted for all types of wires.   Figure 11 shows a soft fault at 8 feet where the connector is located. The signature related to the connector is spread over 2 feet. This is mainly because of the "inductive" nature of the connection, the type of wire (i.e. single), and the relative slow rise-time of the TDR.
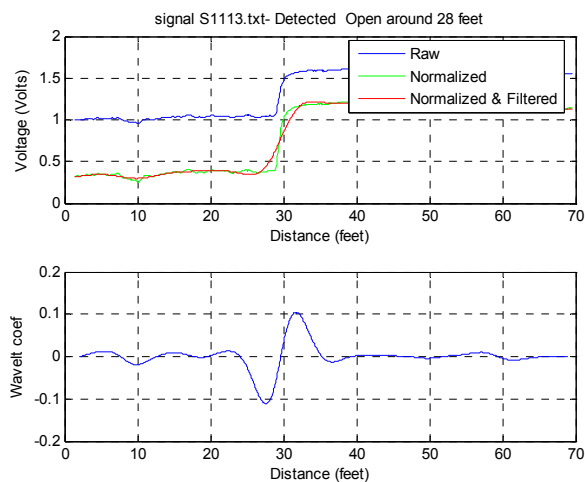
Figure 10. An "open" around 28 feet is detected in a harness made of two single wire-bundles (i.e. 10 feet + 20 feet) connected via a connector.
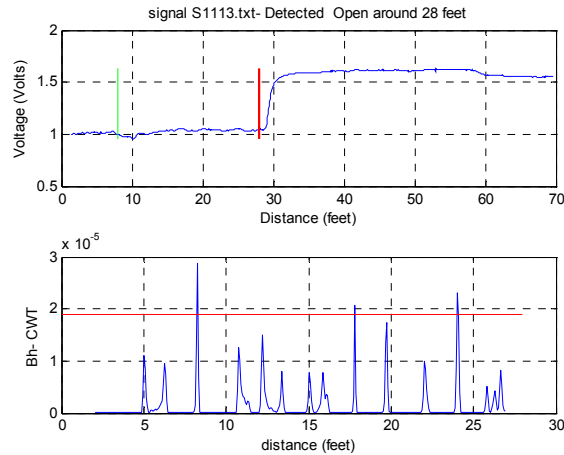
Figure 11. "Soft" defect detected around 8 feet due to the presence of a connector. Soft defects are considered only between the start of the wire and the location of the first "hard" defect, located at 28 feet in this case.

To observe the effect of "wire gauge" and wire type on the system performance, we studied another single wire with a different gauge and a twisted pair of wires. In the previous case (Figures 10-11), the single wire had a gauge of 22. Figure 12 shows the system performance over a single wire of gauge 24. The "open" at the end of the wire (i.e. 29 feet) and the connector around 10 feet are correctly detected in this case. Other measurements over the same wire showed comparable results but location of the "soft" defect (i.e. connector) could not be locked at 10 feet all the times mainly because of the uncontrolled return path in the case of single wires. Figure 13 shows an example of the system performance over a twisted pair. As expected, the system performed better given the controlled return path of this type of wires.

The connector was detected in all type of studied wires except for the case of "triple twisted pair" where the connector-related stationarity index did not reach the detection threshold for "soft" defects as shown by Figure 14. This is mainly due to the relatively high cutoff frequency of the low pass filter that is used to eliminate signal artifacts, such as the hardware-related artifact around 24 feet. When the cutoff frequency is lowered down to 62.5 MHZ instead of 125 MHZ, the stationarity index becomes highest around 10 feet where the connector is located, as shown by Figure 15. A different detection threshold needs then to be set in this case for the system to correctly detect the "soft" defect (i.e. connector). The cutoff frequency of 125 MHZ was chosen as a tradeoff across all types of wires.

Overall, the system performed well over all types of studied wires at Goodrich lab. The studied data set included coax, twisted pair, twisted shielded pair, triple twisted pair, triple twisted shielded pair, and single wires. In all these cases, the end of the wire (i.e. open) was correctly identified around 29 feet. The connector was identified in all types of wires except for the unique case of triple twisted shielded pair mainly due the filtering process that is set to accommodate all types of wires. If one relaxes the restriction of having same parameters for all types of wires the system performance over triple twisted shielded wires and over other types of wire is expected to improve.

As for insulation defects over single wires, as shown by Figures 5-6, the system correctly detected the "soft" defect at 5 feet in all studied cases over a 10-foot wire ahrness. In some occasions, we registered some "false" positives (e.g. Figure 6) in addition to the defect of interest.

5.2. **Sandia lab data**

Several TDR waveforms for "healthy" and "damaged" wires were collected using the GWIT during the visit to the AANC facility in Albuquerque NM, as part of this project. The same algorithms settings and parameters used for the previous set of Goodrich data are used in the case of AANC (Sandia Lab) data for

verification and validation. Figures 16 a-c show examples of the system performance in presence of non damaged wires. The return path in the case of single wires is set to the next pin of the wire of interest. In the case of other types of wires, the return path is the appropriate collocated pair of wire. Figures 16 a-b, correctly identify no "soft" defects in the tested wires. In the case of "single" wire, false positive can happen, as shown by Figure 16-c, but are not common.

Figures 17 a-f show examples of the system performance over a myriad of damaged wires as described in Table I. The system performed well on certain types of damages including defects of types DT1, DT2, DT6, and DT7. This is expected because these defects alter to the wire impedance to a certain degree depending on the severity of the defect and the type of wire. The system performed rather poorly on defects of type DT3, DT5 and DT8. These defects affect mainly the wire insulation or the plastic "coating" of the wire and not the conductors.

5.3. **Aircraft data**

Figures 18 a-d show examples of the system performance over TDR data collected at the Boeing 737 aircraft located at the FAA Tech Center. There are "easy" cases when the system correctly detect and locate "shorts" and "opens", such as the case shown at Figure 18 a. In some other instances, such as the cases shown at Figures 18 b-d, the system detects an "open" but verification needs to be done to assess the natures of these defects. Apparently, in addition to the "short" at the end of the wire of pin "a" around 19 feet and the "open" at the end of wire of the pin "b", there are two "soft" defects around 15 and 9 feet, respectively. Figure 18 c suggests an "open" around 10 feet in the wire of pin "w" but the TDR profile, may suggest a termination of the wire by a high resistive load. Physical inspection of these wire harnesses at the 737 aircraft needs to be done to verify these assertions.

6. Conclusions

Application of joint Time-Frequency techniques has shown promise for wire diagnostics. Continuous Wavelet Transform (CWT) is used to provide joint Time-Frequency Representations (TFRs) of TDR signatures where signal artefacts are well captured both in time and frequency. A Stationarity Index was used to detect signal nonstationarities that are correlated with wire defects. These time-frequency techniques were tested over various types of wires using the Goodrich Wire Integrity Tool (GWIT), a hand held TDR of 200 Pico second rise time and 2.5 GHZ bandwidth. Three different locations were used to collect data subject of this study. Data was collected at the Goodrich engineering lab in Vermont, at Sandia Lab in New Mexico, and over a Boeing 737 airplane at the FAA Tech Center in New Jersey.

The only input to the proposed detection scheme is the TDR waveform. No other properties of the wire are required such as wire type, gauge or length.

The system was tested over 103 data files corresponding to different types of wires, including the challenging type of single wires. Almost half of these data files (i.e. 43 data files) correspond to healthy non-damaged wires. The system correctly detected and located all "hard" defects (i.e. "open" or "short"). Detecting "hard" defects in single wires is not by any means a simple task. The system also detected about half of the "soft" defects and missed the other half. Of the 43 cases of "healthy" wire, only 6 cases (i.e. 14%) were wrongly mischaracterized as being damaged wires. This is a very encouraging result given the fact that the overwhelming majority of studied wires are of type single, which is a very challenging case to diagnose. Published literature addresses mostly well-behaved types of wires with controlled return paths such as coaxial wires and twisted pairs.

The proposed algorithmic approach has been coded and migrated to the Goodrich Wire Integrity Tool and provided to the FAA for further evaluation. Other algorithmic improvements are needed to enhance the system performance particularly in the case of single wires, which constitute most of

aircraft wires. Defining and estimating an "equivalent" distance between the wire and its return path and considering a "2-stimuli" TDR to establish a "live" baseline are two appealing venues for improvements.

7. References

[1] Sadok, M, Huang, N, and Walz, M, "The Hilbert Huang Transform for Wire Diagnostics in Aircraft", 9th Joint FAA/DoD/NASA Aging Aircraft Conference. Atlanta, GA. March 6-9, 2006.

[2] C. Lo, C. Furse, "Noise Domain Reflectometry for Wire Fault Location," *IEEE Trans. Electromagnetic Compatibility*, February 2005, pp.97-104

[3] C. Furse, Y. Chung, R. Dangol, M. Nielsen, G. Mabey, R. Woodward, "Frequency Domain Reflectometry for On Board Testing of Aging Aircraft Wiring," *IEEE Trans. Electromagnetic Compatibility*, May 2003, *p.306-315*.

[4] Sadok. M, Amara Boujemaa. R., and Jaidane. M, "A proof of non Robustness of Reference-based TDR Methods for Diagnosis in Single Wires" submitted to the *14th European Signal Processing Conference (EUSIPCO)*, September 4-8, 2006, Florence, Italy.

[5] H. Laurent and C. Don Carli, "Stationarity Index for Abrupt Change Detection in the time-Frequency Plane", *IEEE Signal Processing Letters*, Vol 5, n°2, pp43-45, 1998.

[6] L. Cohen, "Time Frequency Distributions – A review", *Proceedings of IEEE*, Vol 77, n°7, 1989.

[7] Larbi, S.D, Jaïdane-Saïdane, M, "Audio Watermarking : a Way to Stationarize Audio Signal", IEEE Trans. on Signal Processing, Volume 53, Issue 2, Part 2, pp.816 – 823, Feb. 2005

[8] S. Mallat, "A Theory for Multiresolution Signal Decomposition: The Wavelet Representation," *IEEE Transactions on Pattern Analysis and Machine Intelligence,* Vol. 11, No. 7, pp. 674-693, July 1989.

[9] Dinallo M., and Schneider L., "Aircraft wire systems test bed for use in development of wire-condition measurement technologies", *6th Joint FAA/DoD/NASA Aging Aircraft Conference –* Sept.16-19, 2002

8. Acknowledgment
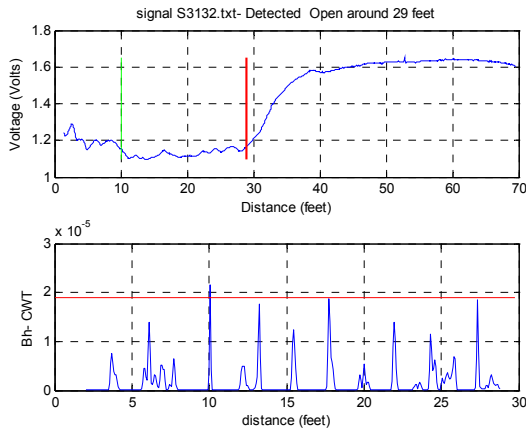
Figure 12. System performance over another pair of single wires . Both end of the wire and connecter are correctly identified.
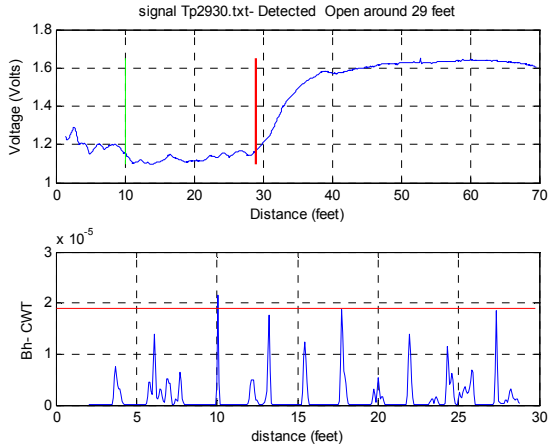

Figure 13. . Example of the system performance over twisted pair.
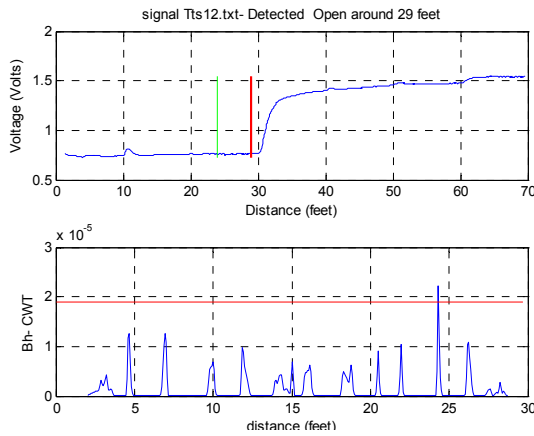

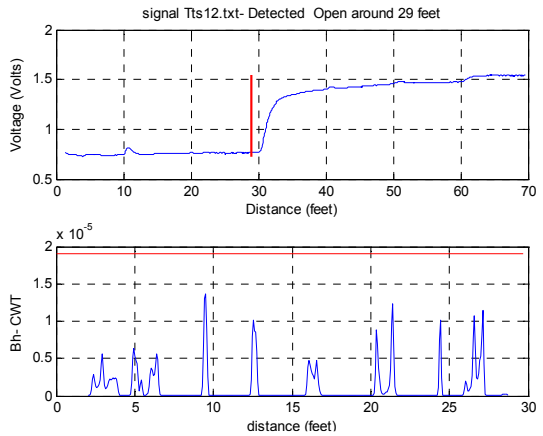**Figure 14. System performance over a triple twisted shielded pair of wires.**

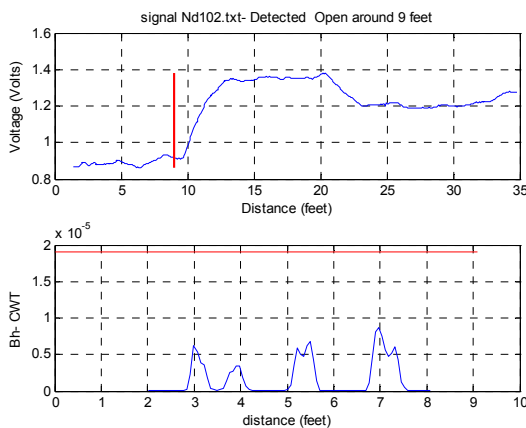**Figure 15. Performance over a triple twisted shielded pair but with lower cutoff frequency**

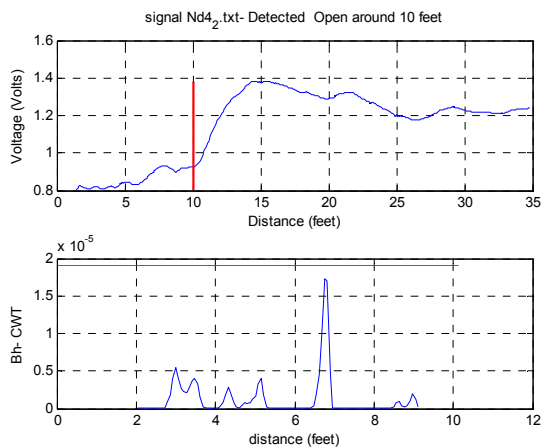**Figure 16a. System performance over a non damaged twisted-pair. The system correctly identifies no defect.**

Figure 16b. System performance over a non damaged single wire.
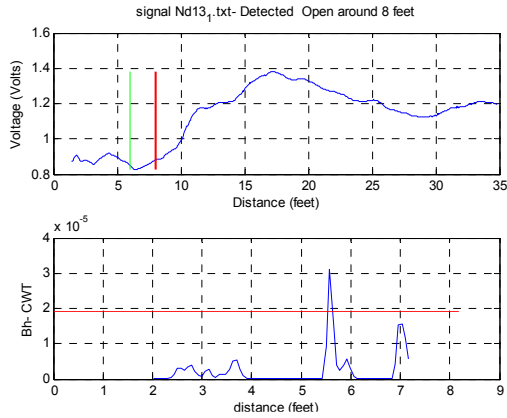
Figure 16c. System performance over a non damaged single wire. The system wrongly identifies a positive at 6 feet..
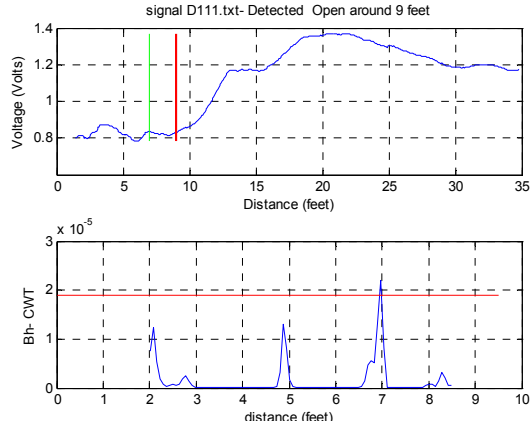
Figure 17a. performance over a damaged twisted pair by a severe breached insulation (defect type DT2). The system correctly detected and located the defect at 7 feet
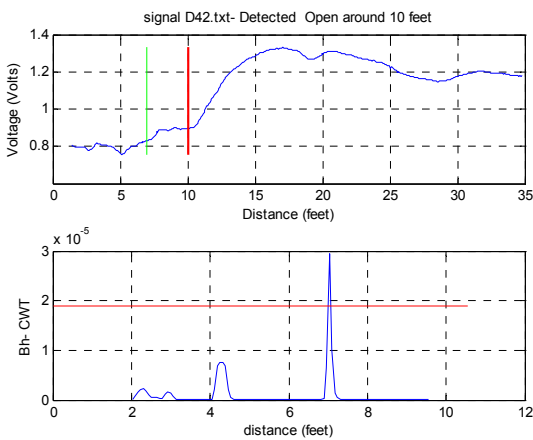
Figure 17b. System performance over a damaged single wire by a faulted splice (defect type DT7). The system correctly detected and located the defect at 7 feet
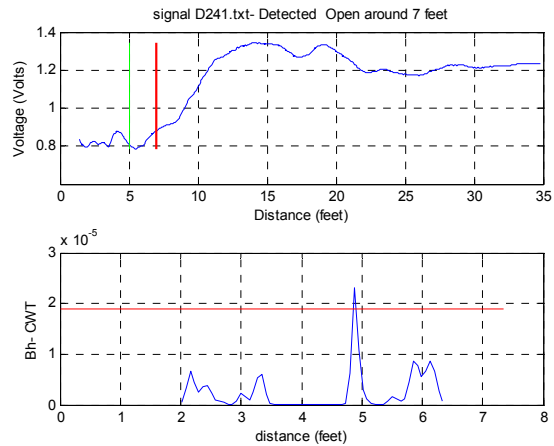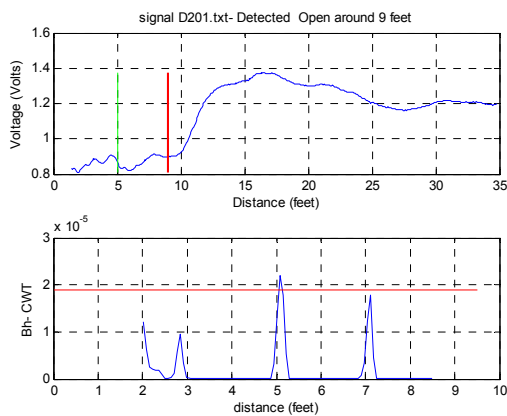
Figure 17c. System performance over a damaged single wire by a wire to ground with 3-millimetr-gap (defect type DT1). The system correctly detected and located the defect

Figure 17d. System performance over a damaged single wire by severely bending the wire 180 degrees (defect type DT6). The system correctly detected and located the defect at 5 feet
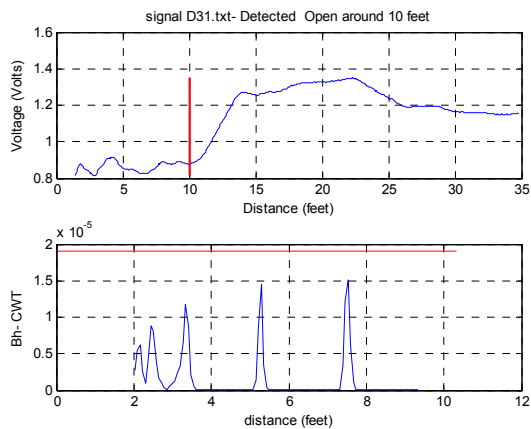
Figure 17e. System performance over a damaged single wire by a cracked insulation (defect type DT3). The system missed the defect at 3 feet

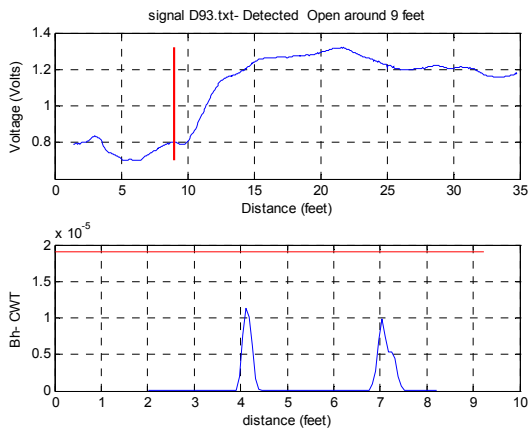Sadok et al., 9th Joint FAA/DoD/NASA Aging Aircraft Conference

Figure 17f. . System performance over a "damaged" single wire by an over-pressured clamp at 100inch/lbs (defect type DT5). The system missed the defect detection at 8 feet
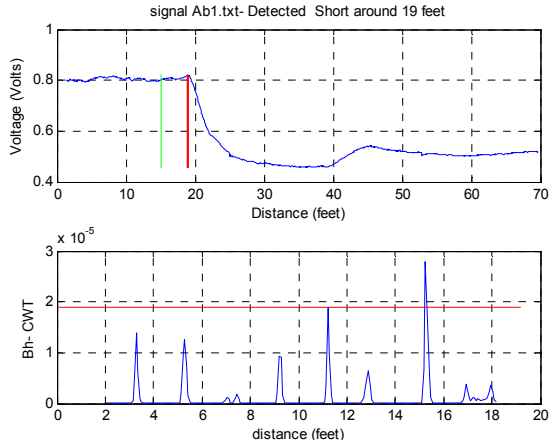

Figure 18a. System performance over the wire of pin "a" of the 737 aircraft. The system indicated a "short" at 19 feet and a "soft" defect at 15 feet
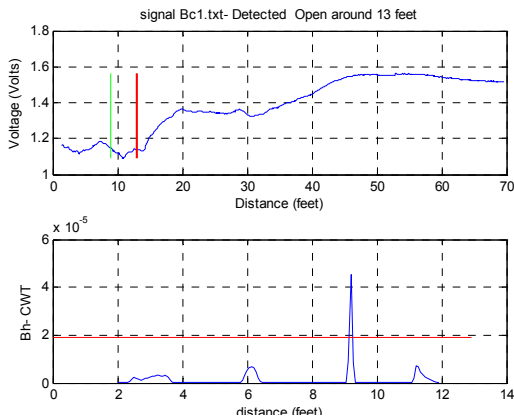

Figure 18b. System performance over a tested wire of the 737 aircraft. The system indicated an "open" defect at 13 feet and a "soft" defect at 9 feet.
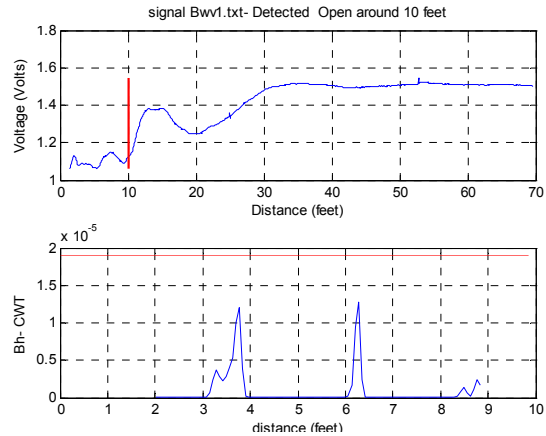

Figure 18c. System performance over a tested wire of the aircraft. The system indicated an "open" at 10 feet; a high resistive load is also a possibility.